Observation of Atomic Diffusion at Twin-Modified Grain Boundaries in Copper

Kuan-Chia Chen *et al.*

Science **321**, 1066 (2008);
DOI: 10.1126/science.1160777

tightly focused laser beams L_1 and L_2 preferentially transfers molecules in the center of the sample and is hence responsible for some selection in velocity space.

It should now be possible to add a second STIRAP step for transfer into the rovibrational ground state $v = 0$, $J = 0$. A suitable two-photon transition at readily available laser wavelengths is via the 68th excited state level of the 0_u^+ potential near 1329 nm (up) and 991 nm (down) with comparatively good wave function overlap at the level of $|\Omega/\Omega_a|^2 \approx 10^{-4}$. We expect that searching for dark resonances will be straightforward, as now all two-photon transition energies are known with an uncertainty of 10^{-3} cm^{-1}. Molecules in $v = 0$, $J = 0$ cannot further decay into a lower state upon a two-body collision, and they are thus expected to allow the formation of an intrinsically stable molecular BEC. The high speed of our STIRAP transfer will allow us to perform in situ as well as time-of-flight imaging for direct characterization of the spatial and momentum distribution of the molecular ensemble.

With our technique, any low-lying vibrational state can be coherently populated in a controlled fashion with full control over the rotational quantum number, allowing, for instance, state-specific collisional studies and high-precision molecular spectroscopy with possible implications for fundamental physics (*6*, *7*). Our procedure can be adapted to other species, in particular to heteronuclear alkali dimers such as RbCs (*25*) and KRb (*15*) for the creation of dipolar quantum gases (*26*). For heteronuclear alkali dimers, a single two-photon transfer step might suffice as a result of favorable wave function overlap (*27*). We expect that the combination of our technique with Feshbach molecule production out of a Mott-insulator state in a three-dimensional lattice (*28*) will increase the initial Feshbach molecule production efficiency, avoiding collective excitations as a result of magnetic field ramping and inhibiting collisional loss, and will provide full control over all internal and external quantum degrees of freedom of the ground state molecules.

References and Notes

1. C. Chin *et al.*, *Phys. Rev. Lett.* **94**, 123201 (2005).
2. T. Kraemer *et al.*, *Nature* **440**, 315 (2006).
3. P. Staanum, S. D. Kraft, J. Lange, R. Wester, M. Weidemüller, *Phys. Rev. Lett.* **96**, 023201 (2006).
4. N. Zahzam, T. Vogt, M. Mudrich, D. Comparat, P. Pillet, *Phys. Rev. Lett.* **96**, 023202 (2006).
5. R. V. Krems, *Int. Rev. Phys. Chem.* **24**, 99 (2005).
6. T. Zelevinsky, S. Kotochigova, J. Ye, *Phys. Rev. Lett.* **100**, 043201 (2008).
7. D. DeMille *et al.*, *Phys. Rev. Lett.* **100**, 043202 (2008).
8. M. Inguscio, W. Ketterle, C. Salomon, Eds., *Ultracold Fermi Gases, Proceedings of the International School of Physics "Enrico Fermi," Course CLXIV* (IOS Press, Amsterdam, 2008).
9. D. DeMille, *Phys. Rev. Lett.* **88**, 067901 (2002).
10. J. Doyle, B. Friedrich, R. V. Krems, F. Masnou-Seeuws, *Eur. Phys. J. D* **31**, 149 (2004).
11. T. Köhler, K. Góral, P. S. Julienne, *Rev. Mod. Phys.* **78**, 1311 (2006).
12. K. M. Jones, E. Tiesinga, P. D. Lett, P. S. Julienne, *Rev. Mod. Phys.* **78**, 483 (2006).
13. D. Jaksch, V. Venturi, J. I. Cirac, C. J. Williams, P. Zoller, *Phys. Rev. Lett.* **89**, 040402 (2002).
14. K. Winkler *et al.*, *Phys. Rev. Lett.* **98**, 043201 (2007).
15. S. Ospelkaus *et al.*, preprint available at http://arxiv.org/abs/0802.1093 (2008).
16. T. Weber, J. Herbig, M. Mark, H.-C. Nägerl, R. Grimm, *Science* **299**, 232 (2003), published online 5 December 2002; 10.1126/science.1079699.
17. J. Herbig *et al.*, *Science* **301**, 1510 (2003), published online 21 August 2003; 10.1126/science.1088876.
18. M. Mark *et al.*, *Phys. Rev. A* **76**, 042514 (2007).
19. K. Bergmann, H. Theuer, B. W. Shore, *Rev. Mod. Phys.* **70**, 1003 (1998).
20. W. Weickenmeier *et al.*, *J. Chem. Phys.* **82**, 5354 (1985).
21. C. Amiot, O. Dulieu, *J. Chem. Phys.* **117**, 5155 (2002).
22. Laser L_1 near 1126 nm and laser L_2 near 1006 nm are continuous-wave grating-stabilized tunable diode lasers with up to 26 mW and 5 mW of power at the sample position, respectively, both focused to a $1/e^2$ waist of ~25 μm for sufficiently high Rabi frequencies. We estimate the laser linewidth for both lasers to be on the order of 1 kHz. The laser beams propagate horizontally at an angle of 80° with the long axis of the BEC with vertical linear polarization. Copropagation assures that the imparted photon recoil during STIRAP is minimal, corresponding to an energy of $k_B \times 0.4$ nK, with Boltzmann's constant k_B. The beam intensity is controlled by acousto-optical modulators, allowing pulse lengths down to 1 μs.
23. The wave-meter calibration is currently not sufficient to allow absolute numbering of the frequency comb teeth.
24. T. Kraemer *et al.*, *Appl. Phys. B* **79**, 1013 (2004).
25. J. M. Sage, S. Sainis, T. Bergeman, D. DeMille, *Phys. Rev. Lett.* **94**, 203001 (2005).
26. K. Góral, L. Santos, M. Lewenstein, *Phys. Rev. Lett.* **88**, 170406 (2002).
27. W. C. Stwalley, *Eur. Phys. J. D* **31**, 221 (2004).
28. T. Volz *et al.*, *Nat. Phys.* **2**, 692 (2006).

29. We thank the team of J. Hecker Denschlag, the LevT team in our group, and T. Bergeman for very helpful discussions and M. Prevedelli for technical assistance. We are indebted to R. Grimm for generous support and gratefully acknowledge funding by the Austrian Ministry of Science and Research (Bundesministerium für Wissenschaft und Forschung) and the Austrian Science Fund (Fonds zur Förderung der wissenschaftlichen Forschung) in the form of a START prize grant and by the European Science Foundation in the framework of the EuroQUAM collective research project QuDipMol.

1 May 2008; accepted 1 July 2008
Published online 10 July 2008;
10.1126/science.1159909
Include this information when citing this paper.

Observation of Atomic Diffusion at Twin-Modified Grain Boundaries in Copper

Kuan-Chia Chen,[1]* Wen-Wei Wu,[2]* Chien-Neng Liao,[1]† Lih-Juann Chen,[1] K. N. Tu[3]

Grain boundaries affect the migration of atoms and electrons in polycrystalline solids, thus influencing many of the mechanical and electrical properties. By introducing nanometer-scale twin defects into copper grains, we show that we can change the grain-boundary structure and atomic-diffusion behavior along the boundary. Using in situ ultrahigh-vacuum and high-resolution transmission electron microscopy, we observed electromigration-induced atomic diffusion in the twin-modified grain boundaries. The triple point where a twin boundary meets a grain boundary was found to slow down grain-boundary and surface electromigration by one order of magnitude. We propose that this occurs because of the incubation time of nucleation of a new step at the triple points. The long incubation time slows down the overall rate of atomic transport.

Grain boundaries affect many physical properties of polycrystalline solids. For example, reduction of grain size is known to improve the mechanical strength of metals, governed by the Hall-Petch equation (*1*, *2*). A large-angle tilt-type grain boundary can short-circuit atomic diffusion, which has been the most serious reliability issue in Al interconnects in microelectronics technology. The atomic structure of a grain boundary is controlled by the misorientation between the two grains forming the grain boundary. Balluffi *et al.* have made bicrystals of Au thin films and varied systematically the tilt or twist angle in the bicrystals for studying the correlation between formation energy and atomic structure of grain boundaries (*3*, *4*). Generally speaking, the higher the grain-boundary misorientation angle, the higher the atomic diffusivity. Thus, by modifying the structure of a grain boundary, it should be possible to control the atomic diffusion along the grain boundary.

Lu *et al.* have synthesized a high density of nanotwins in pure Cu foils by pulsed electrodeposition (*5*). The average grain size in the Cu foils is ~400 nm, and the high-density twins have a peak at 15 nm in twin-lamella size distribution. The Cu foil shows a 10-fold improvement of the mechanical strength relative to a large-grained Cu, and the foil remains ductile but its electrical resistance did not significantly change. High mechanical strength and low electrical resistivity are desired properties for interconnecting wires in integrated circuits from the consideration of the resistive-capacitive delay, electromigration (EM), and stress migration (*6*–*8*). EM is enhanced

[1]Department of Materials Science and Engineering, National Tsing Hua University, Hsinchu 30013, Taiwan, Republic of China. [2]Department of Materials Science and Engineering, National Chiao Tung University, Hsinchu 30010, Taiwan, Republic of China. [3]Department of Materials Science and Engineering, University of California, Los Angeles, CA 90095, USA.

*These authors contributed equally to this work.
†To whom correspondence should be addressed. E-mail: cnliao@mx.nthu.edu.tw

atomic diffusion under a high-density electric current. Stress migration is creep and is atomic diffusion driven by a normal stress-potential gradient. With the increase in density of electric current in integrated circuits, EM-induced voids and hillocks in conductors can lead to circuit reliability failure (*9*). EM-induced mass transport, in principle, can take place along different diffusion paths such as lattices, grain boundaries, surfaces, and interfaces (*10*, *11*). It is now generally accepted that free surfaces or interfaces are principal EM paths in Cu interconnects at the device operation temperature ~100°C, and grain boundaries become preferential EM paths at high temperatures (*12*). Conventional EM investigations of interconnects were conducted by measuring the changes in electrical resistance or monitoring morphological changes due to void or hillock formation in the current-stressed metal lines (*13*, *14*). The mass transport can be observed indirectly by marker displacement (*15*). However, no direct observations of EM-induced atomic-scale mass transport have been conducted.

To study atomic-scale EM in the nanotwin modified grain boundaries requires in situ high-resolution transmission electron microscopy (HRTEM) and ultrahigh vacuum to prevent oxidation of the Cu under high temperature and high current. Our previous studies of Cu have revealed that the EM-induced mass transport occurs preferentially on the {111} surface planes and along the <110> directions, leading to a unique stepped atomic-surface structure in crystalline Cu (*16*, *17*). In the present study, we introduced nanotwins into the test samples of Cu (*18*). The specimens for in situ TEM observation were prepared through conventional thin-film deposition and patterning processes (fig. S1, A to E). A scanning electron micrograph of the test specimen around the observation window is shown in fig. S1F.

Figure 1 shows a set of HRTEM images of a twin-modified grain boundary at different stages during electric current stressing. A twin lamella has two twinning planes, so it will intersect a grain boundary with two triple points. Because a grain boundary is formed by two grains, we should have twins to intersect the grain boundary from both sides. We inspected only one of the two grains forming the grain boundary: the grain in the lower part of the image, which is $(01\bar{1})$-oriented or has $[01\bar{1}]$ as the surface normal. This grain has several {111}/<112>–type coherent twin boundaries that appear to have an angle of 70.5° with respect to the (111) lattice planes. Under the influence of EM, the edge of this $(01\bar{1})$-oriented grain in the grain-boundary plane has evolved into a zigzag shape. The zigzag edges in the grain boundary were found to be $(1\bar{1}\,\bar{1})$ and $(4\bar{2}\bar{2})$ atomic planes that are separated by the thickness of the twin lamellae, as shown in Fig. 1, A to D.

The direction of electron flux is from the right to the left of the inspected grain. We observed that an atomic step appeared at the triple point of the twin boundary (TB1) in Fig. 1 and moved rather rapidly on the $(1\bar{1}\,\bar{1})$ plane toward the other triple point of the twin boundary (TB2). The results indicate that the Cu atoms move on the $(1\bar{1}\,\bar{1})$ surface along the direction of electron flux (from right to left), resulting in the atomic step moving in the opposite direction. Once the atomic step reached TB2, we observed that it was trapped for a while before moving out onto the $(4\bar{2}\bar{2})$ plane. Movie S1 shows the atomic-step movement and the effect of the twin boundary on slowing down EM (*18*). By tracing the atomic steps moving along the $(1\bar{1}\,\bar{1})$ and $(4\bar{2}\bar{2})$ facet surfaces, we can plot the distances of different atomic steps from TB1 and TB2, with respect to time, as shown in Fig. 2. We found that there exists a time lag of ~5 s for the atomic steps to cross the triple points under electric current stressing with an average current density of 2.5×10^6 A/cm^2. The moving speeds of the atomic steps on the $(1\bar{1}\,\bar{1})$ and $(4\bar{2}\bar{2})$ surfaces were calculated to be 5.7 ± 0.4 and 3.4 ± 0.3 nm/s, respectively, based on the plots in Fig. 2, A and B. Because the {111} crystal planes have the lowest atomic-migration energies among the major low-index planes in Cu, it would not be surprising to find that the moving speed of atomic steps on the $(1\bar{1}\,\bar{1})$ surface is faster than that on the $(4\bar{2}\bar{2})$ surface (*19*). Nevertheless, the most important finding is that the triple points can slow down or block the EM-induced atomic migration in the twin-modified grain boundaries of Cu.

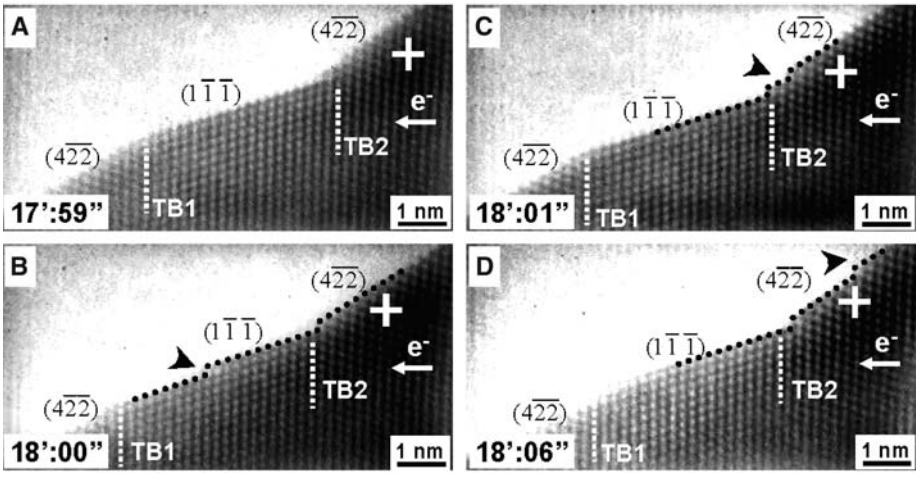

Fig. 1. (**A** to **D**) HRTEM images of the $(01\bar{1})$-oriented Cu grain under electric current stressing as a function of time. The time of the image capture (in minutes and seconds) is given in the rectangular box at the lower left corner. The direction of electron flow is from right to left. The arrowheads indicate the atomic steps on the lattice planes. The cross in each panel refers to a fixed point for ease of inspection. The HRTEM image was analyzed by fast Fourier transform technique.

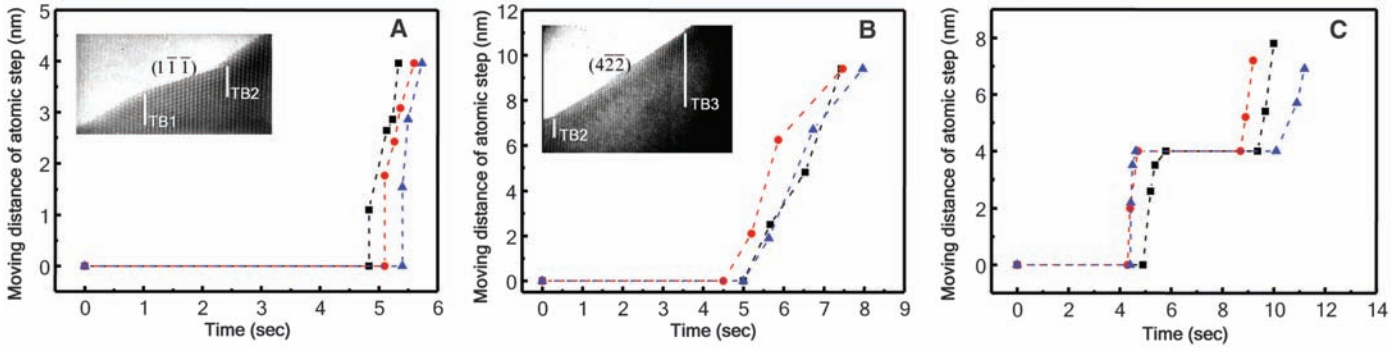

Fig. 2. Movement of different atomic steps on (**A**) the $(1\bar{1}\,\bar{1})$ surface, (**B**) the $(4\bar{2}\bar{2})$ surface, and (**C**) the surface between TB1 and TB3 as a function of time. Insets in (A) and (B) show the moving trace of the atomic steps. Black squares, atomic step 1; red circles, atomic step 2; blue triangles, atomic step 3.

Now the question is why can the triple points of twin boundaries block the EM-induced atomic diffusion? In general, atoms are released from a kink site on a stepped surface of $(1\bar{1}\,\bar{1})$ and $(4\bar{2}\bar{2})$ planes. At a triple point, if we assume that the atomic arrangement is close to a coincidence site, it is energetically less favorable to form a step and kink site at the triple points. More importantly, in a transition from a $(1\bar{1}\,\bar{1})$ to a $(4\bar{2}\bar{2})$ surface, for example, the nucleation of a new step and a kink site on the $(4\bar{2}\bar{2})$ surface is required, so an incubation time is also needed. Overall, the nucleation of steps from the triple points would be the rate-limiting step, resulting in a time lag for the atomic diffusion across the triple points, as shown in Fig. 2, A and B. When we recorded the atomic step moving along the facet surfaces and plotted the moving distance of an atomic step as a function of time, we found a stair-type curve, as shown in Fig. 2C. We interpret that the horizontal part of a step is the incubation time spent to nucleate a new step on the $(1\bar{1}\,\bar{1})$ or $(4\bar{2}\bar{2})$ surface, and the vertical part of a step is the propagation or growth of the step across the $(1\bar{1}\,\bar{1})$ or $(4\bar{2}\bar{2})$ surface. We obtained similar stair-type curves when we followed EM along the grain boundary over several triple points.

With the Cu atoms continuously drifting away under electric current stressing, the atomic steps in the $(01\bar{1})$-oriented grain were found to disappear gradually, and a void eventually formed along the entire grain boundary. This is because EM-induced grain-boundary diffusion is nonconservative (*20*). As it is an irreversible process, we cannot assume vacancy to be at equilibrium everywhere in the sample. Figure 3 shows a set of schematic diagrams of the grain boundary and twin boundaries of one of the Cu grains with $(01\bar{1})$ crystal planes parallel to the surface of the Cu line sample at different stages during electric current stressing. The HRTEM images were obtained from a local spot of the inspected Cu grain to highlight the evolution of the atomic-scale EM-induced voiding along the grain boundary. We found that the atomic steps gradually vanished from the upper left corner of the grain in Fig. 3A. With time, the void grows to the right against the electron-flow direction and also grows downward. The upper free surface of the void is the original grain-boundary plane on the top side, and the lower free surface of the void becomes a zigzag type of free surface consisting of $(1\bar{1}\,\bar{1})$ and $(4\bar{2}\bar{2})$ edges of twins, as shown in Fig. 3, B and C. The size of the void was ~10 to 20 nm wide. Finally, the whole grain almost completely disappeared after electrically stressing the specimen for 30 min, as revealed in Fig. 3D.

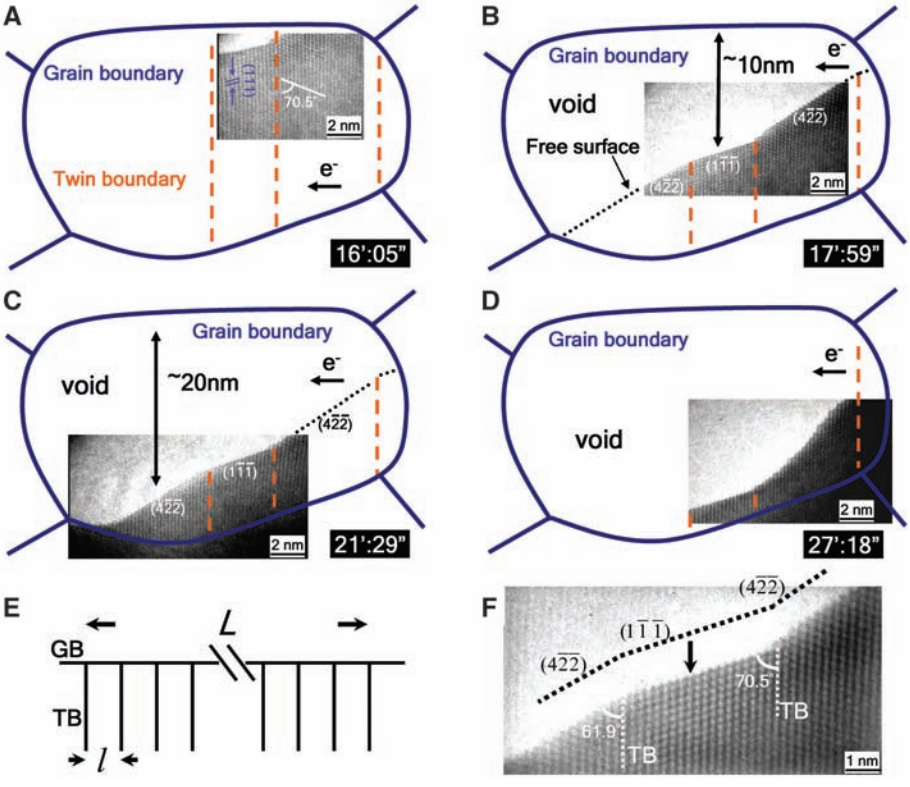

Fig. 3. Schematic diagrams of the grain boundary and twin boundaries of a $(01\bar{1})$-oriented Cu grain at different stages during electric current stressing. (**A** to **D**) Time of the HRTEM image capture is given (in minutes and seconds) in the rectangular box at the lower right corner. The direction of electron flow is from right to left. (**E**) Cartoon of a twin-structured Cu grain of dimension *L* with an average twin-lamella width of *l*. GB, grain boundary; TB, twin boundary. Arrows indicate the span of the Cu grain and twin lamella. (**F**) HRTEM image of the grain edge revealing the direction of EM-induced voiding (indicated by the downward arrow).

In dual-damascene Cu interconnect technology, surface and interfaces have been found to be the dominant kinetic paths of EM in device operation temperature. It is generally accepted that grain boundaries become the more active EM paths for copper when the surface and interfacial paths are blocked or if the temperature reaches above 300°C (*12*). However, as a void is formed (Fig. 3), surface diffusion occurs. We have performed an independent experiment to measure the heating of the Cu specimen induced by the transmission electron beam with the use of a thermocouple attached to the TEM specimen holder, and we found no significant temperature rise for the specimen exposed to the electron beam for 3 hours. One may argue that the local temperature of the specimen due to electron-beam heating might be much higher than the overall temperature measured. In fact, we also found lots of EM-induced grain-boundary voids elsewhere in the specimen without direct electron-beam exposure. This observation indicates that the observed EM-induced voiding is not directly affected by the electron-beam heating. If the electron-beam heating is not severe, it seems that grain-boundary diffusion in large-angle grain boundaries can still be active EM paths at low temperatures.

The measured speed of a moving atomic step and the triple point–induced incubation time lag can be used to evaluate the kinetics of EM-induced voiding in the twin-modified Cu. Figure 3, E and F, shows a schematic of a twin-modified Cu grain of dimension L with an average twin-lamella width of l and a HRTEM image of the grain edge with a zigzag feature. Surface diffusion becomes the active EM path once the void is formed in the upper part of the image, as shown in Fig. 3F. We can calculate the time (t_{tw}) required to remove a layer of Cu atoms from the edge of the twin-modified grain as follows

$$t_{tw} = \frac{L}{l} \times 5 + \frac{(L/2)\csc(70.5^\circ)}{v_{\{111\}}} + \frac{(L/2)\csc(61.9^\circ)}{v_{\{422\}}} \quad (1)$$

where $v_{\{111\}}$ and $v_{\{422\}}$ are the moving speeds of atomic step on the {111} and {422} crystal planes, respectively, and L and l are the grain size and twin-lamellar thickness, respectively. In the right-hand side of the equation, the 5 in the first term reflects the delay time of 5 s associated with each triple point of the twin boundaries, whereas the second and third terms account for the time of the atomic step moving along the {111} and {422} facets, respectively. Equation 1 is established with the reasonable assumption that the twinned region is approximately equal in extent to the untwinned region in the grain. On the other hand, the time required to remove an atomic layer from a twin-free Cu grain of dimension L will be $t_0 = [L\csc(70.5^\circ)]/v_{\{111\}}$, because the {111} planes are the most favorable EM surfaces. The EM-induced void is expected to grow in the direction normal to the facets with a rate that is inversely

proportional to the above estimated time (t_{tw} and t_0). With the measured $v_{\{111\}}$ and $v_{\{422\}}$ values, the EM-induced void growth rate for the twin-modified Cu grain (l = 5 nm) is calculated to be approximately one order of magnitude lower than that for the twin-free Cu grain. The effect of twin boundaries on slowing down the EM-induced voiding is expected to decrease with an increase of the twin-lamella width (that is, a decrease in the twin density). The twin boundary–induced atomic-migration delay may also decrease with rising temperature because the EM-induced atomic diffusion is a thermally activated process. However, typical integrated circuit devices usually operate at temperatures ~100°C.

We have observed the atomic-scale EM process in twin-modified Cu grains near room temperature with the use of ultrahigh-vacuum and high-resolution TEM technique. The EM-induced atomic migration along a twin-modified grain boundary was observed, and the presence of the triple point of a coherent twin boundary meeting a grain boundary was found to retard the EM-induced atomic transport.

References and Notes

1. E. O. Hall, *Proc. Phys. Soc. London Sect. B* **64**, 747 (1951).
2. N. J. Petch, *J. Iron Steel Inst. London* **174**, 25 (1953).
3. R. W. Balluffi, R. F. Mehl, *Metall. Mater. Trans. A* **13**, 2069 (1982).
4. S. W. Chan, R. W. Balluffi, *Acta Metall.* **33**, 1113 (1985).
5. L. Lu, Y. Shen, X. Chen, L. Qian, K. Lu, *Science* **304**, 422 (2004), published online 18 March 2004; 10.1126/science.1092905.
6. C. K. Hu, J. M. E. Harper, *Mater. Chem. Phys.* **52**, 5 (1998).
7. R. Frankovic, G. H. Bernstein, *IEEE Trans. Electron. Dev.* **43**, 2233 (1996).
8. P. Børgesen, J. K. Lee, R. Gleixner, C. Y. Li, *Appl. Phys. Lett.* **60**, 1706 (1992).
9. I. A. Blech, *J. Appl. Phys.* **47**, 1203 (1976).
10. C. K. Hu, R. Rosenberg, K. Y. Lee, *Appl. Phys. Lett.* **74**, 2945 (1999).
11. C. S. Hau-Riege, *Microelectron. Reliab.* **44**, 195 (2004).
12. K. N. Tu, *J. Appl. Phys.* **94**, 5451 (2003).
13. J. S. Huang, T. L. Shofner, J. Zhao, *J. Appl. Phys.* **89**, 2130 (2001).
14. E. Liniger, L. Gignac, C. K. Hu, S. Kaldor, *J. Appl. Phys.* **92**, 1803 (2002).
15. C. K. Hu, K. Y. Lee, L. Gignac, R. Carruthers, *Thin Solid Films* **308-309**, 443 (1997).
16. C. N. Liao, K. C. Chen, W. W. Wu, L. J. Chen, *Appl. Phys. Lett.* **87**, 141903 (2005).
17. K. C. Chen, C. N. Liao, W. W. Wu, L. J. Chen, *Appl. Phys. Lett.* **90**, 203101 (2007).
18. See supporting material on *Science* Online.
19. M. Karimi, T. Tomkowski, *Phys. Rev. B* **52**, 5364 (1995).
20. A. P. Sutton, R. W. Balluffi, in *Interfaces in Crystalline Materials* (Clarendon Press, Oxford, 1995), chap. 10, p. 598.

21. The work was supported by the National Science Council through grants NSC 96-2120-M-007-006 and 96-2628-E-007-018-MY3. K.N.T. acknowledges the support of NSF–Nanoscale Interdisciplinary Research Team contract CMS-0506841.

Supporting Online Material

www.sciencemag.org/cgi/content/full/321/5892/1066/DC1
Materials and Methods
Fig. S1
Movie S1

21 May 2008; accepted 10 July 2008
10.1126/science.1160777

A Stable Silicon(0) Compound with a Si=Si Double Bond

Yuzhong Wang, Yaoming Xie, Pingrong Wei, R. Bruce King, Henry F. Schaefer III, Paul von R. Schleyer,* Gregory H. Robinson*

Dative, or nonoxidative, ligand coordination is common in transition metal complexes; however, this bonding motif is rare in compounds of main group elements in the formal oxidation state of zero. Here, we report that the potassium graphite reduction of the neutral hypervalent silicon-carbene complex L:$SiCl_4$ {where L: is :C[N(2,6-Pr^i_2-C_6H_3)CH]$_2$ and Pr^i is isopropyl} produces L:(Cl)Si–Si(Cl):L, a carbene-stabilized bis-silylene, and L:Si=Si:L, a carbene-stabilized diatomic silicon molecule with the Si atoms in the formal oxidation state of zero. The Si-Si bond distance of 2.2294 ± 0.0011 (standard deviation) angstroms in L:Si=Si:L is consistent with a Si=Si double bond. Complementary computational studies confirm the nature of the bonding in L:(Cl)Si–Si(Cl):L and L:Si=Si:L.

Although silicon is predominantly associated with semiconductors, integrated circuits, and advanced electronic devices, its structures and bonding motifs intrigue chemists because they are often substantially different from those of silicon's lighter congener carbon. For example, the chemical and physical properties of CO_2 are totally unlike those of SiO_2, and hypervalent species such as $[SiF_5]^-$ are unknown for carbon (*1*). Even though molecules containing C-C multiple bonds are ubiquitous and have been studied for more than two centuries, it was not until 1981 that a disilene, a compound containing a Si-Si double bond ($R_2Si{=}SiR_2$, where R is $Me_3C_6H_2$) was prepared by West *et al.* (*2*); a disilyne (RSi≡SiR, where R is an extremely bulky ligand), a compound containing a Si-Si triple bond (albeit with a decidedly nonlinear, transbent geometry), was ultimately achieved by Sekiguchi *et al.* in 2004 (*3*). In addition to disilenes and disilynes, a number of other interesting stable low-coordinate Si compounds have been reported (*4*–*7*). Regarding the oxidation state of Si in low-coordinate compounds, the central Si atoms in disilenes and disilynes are in the formal oxidation states of two (+2) and one (+1), respectively. It is well known for transition metals to assume the formal oxidation state of zero in organometallic compounds [for example, $Ni(CO)_4$, $(C_6H_6)_2Cr$, etc.]; however, the formal oxidation state of zero is rare for main group elements in their compounds (apart from those in Zintl phases) (*8*, *9*).

The study of highly reactive Si(0) intermediates may prove critical in the development of new synthetic strategies in Si chemistry. Such experimental studies, however, require sophisticated instruments and elaborate techniques (*10*). For example, the diatomic Si_2 molecule, having a triplet ground state ($X^3\Sigma_g^-$), has been studied only in the gas phase and in argon matrices (*11*). Recently, the CO complex of the Si_2 molecule, OC:Si=Si:CO, was examined with argon matrix isolation absorption infrared spectroscopy and computed to have an unusual transbent structure

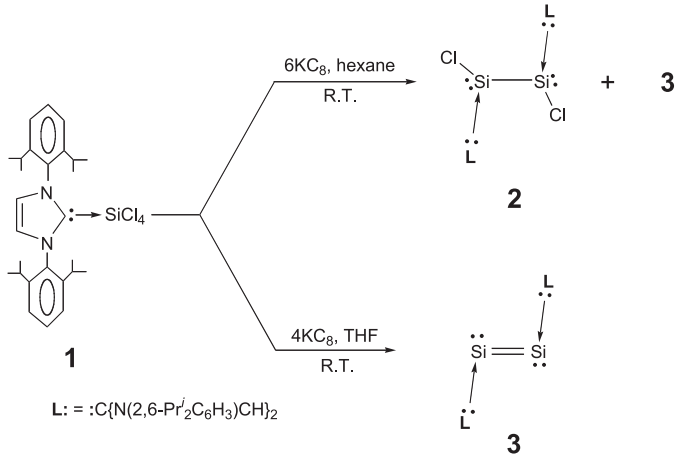

Fig. 1. Synthetic scheme for compounds **2** and **3**.

Department of Chemistry and Center for Computational Chemistry, The University of Georgia, Athens, GA 30602–2556, USA.

*To whom correspondence should be addressed. E-mail: schleyer@chem.uga.edu (P.v.R.S.); robinson@chem.uga.edu (G.H.R.)